Journal of Materials Processing Technology 215 (2015) 1–5

Contents lists available at ScienceDirect

Journal of Materials Processing Technology

journal homepage: www.elsevier.com/locate/jmatprotec

304 stainless steel brazing incorporating tungsten nanoparticles

H.M. Hdz-García[a,*], M.I. Pech-Canul[b,c], R. Muñoz-Arroyo[a], A.I. Mtz-Enriquez[b], J.L. Acevedo-Dávila[a], M.J. Castro-Román[b], F.A. Reyes-Valdés[a]

[a] Corporación Mexicana de Investigación en Materiales S.A. de C.V., Ciencia y Tecnología No. 790, Fracc. Saltillo 400, Saltillo, Coah, CP 25290, Mexico
[b] Cinvestav IPN Unidad Saltillo, Ave. Industria Metalúrgica No. 1062, Parque Industrial Saltillo-Ramos Arizpe, Ramos Arizpe, Coah, CP 25900, Mexico
[c] Cinvestav IPN Zacatenco, Programa de Doctorado en Nanociencias y Nanotecnología (DNN), Av. Instituto Politécnico Nacional 2508, San Pedro Zacatenco, Gustavo A. Madero, 07360 Ciudad de México, Distrito Federal, Mexico

ARTICLE INFO

Article history:
Received 26 March 2014
Received in revised form 31 July 2014
Accepted 1 August 2014
Available online 12 August 2014

Keywords:
Brazing
Nanoparticles
Microstructure
Stainless steel
Vickers hardness

ABSTRACT

Tungsten nanoparticles of 80 nm average particle size were utilized in the brazing of 304 stainless-steels. The nanoparticles were characterized by DTA and TEM, and the brazed samples were evaluated by SEM and Vickers microhardness tests. The interaction of the tungsten nanoparticles with the metallic filler in the melting zone modified the size and morphology of the formed phases into a finer and uniformly distributed microstructure. In samples treated at 1200 °C for 60 min, the microhardness decreased from 310 to 170 HV, being the latter value, close to that of the base metal. The nanoparticles and the microcracks develop a synergistic effect when they are in contact with the liquid phase in such a way that a rise in the threshold capillary-pressure leads to the filling of the interstices. The capillary-like system resulting from the wettability of the nanoparticles and microcrack surfaces by the liquid phase, leads to a solidified microstructure with fine and uniform phase distribution.

1. Introduction

Owing to their excellent properties such as corrosion resistance and optimum hardness at room temperature, stainless steels are essential for medical, chemical, cryogenic containers and biotechnological applications. However, under certain conditions, the brazed stainless steels are susceptible to corrosion, which reduces their mechanical properties and gives place to fracture initiation. Those adverse effects are mainly present near the areas joined by brazing. In the case of micro-cracking with no soldering, that effect is ascribed to an inadequate penetration of the flux used during the brazing process, given the complex path of the microcracks. The foregoing situation can be solved using the transient liquid phase (TLP) bonding, considered as a preferred repairing/joining process for nickel base superalloys due to its ability to produce near-ideal joints, a weld bead with at higher melting point than base metal and free of intermetallics or eutectic phases, as shown by Pouranvari et al. (2009). The main advantage of TLP is the formation of a melt in the interlayer and dissolution of the substrate material in the bond region, as established by Cook and Sorensen (2011). The foremost difference between the brazing and the TLP processes, is that the latter involves four well-defined steps whilst technically, brazing is simply the joining of two base materials with a filler metal, as defined by the AWS (American Welding Society). The four steps of TLP process are as follows: (1) setting up the bond; (2) heating to the specified bonding temperature to produce a liquid in the bond region; (3) holding the assembly at the bonding temperature until the liquid has isothermally solidified due to diffusion and (4) homogenizing the bond at a suitable heat-treating temperature. Sometimes in the TLP process, the dissolution of the substrate is not activated, thus avoiding the isothermal solidification (Cook and Sorensen, 2011). Studies such as that by Philips et al. (2008) have suggested that the microstructural evolution in the weld bead of austenitic stainless steels depends on thermochemical interactions with the parent alloy through dissolution, re-precipitation reactions, and solid-state diffusion during the TLP, but that it can be restricted for wide joints because the dissolution is not sufficient to eliminate the intermetallics. Analytical modeling conducted by Zhou (2001) established that liquid phase is at its maximum width when the isothermal solidification stage starts. Also, Jalilian et al. (2006) showed that at the bonding temperature, the interlayer melts, filling the surface gaps with a thin liquid layer. An advantage can be taken of this liquid phase to fill the micro-cracks and micro-pores by capillary processes between the TLP and the melting filler metal. Byong-Ho and Dae-Up (2002) and Abdelfath

* Corresponding author. Tel.: +52 8442237153; fax: +52 8444113200.
E-mail addresses: hmanuelhdz@comimsa.com, hghm70@hotmail.com (H.M. Hdz-García).

http://dx.doi.org/10.1016/j.jmatprotec.2014.08.001
0924-0136/

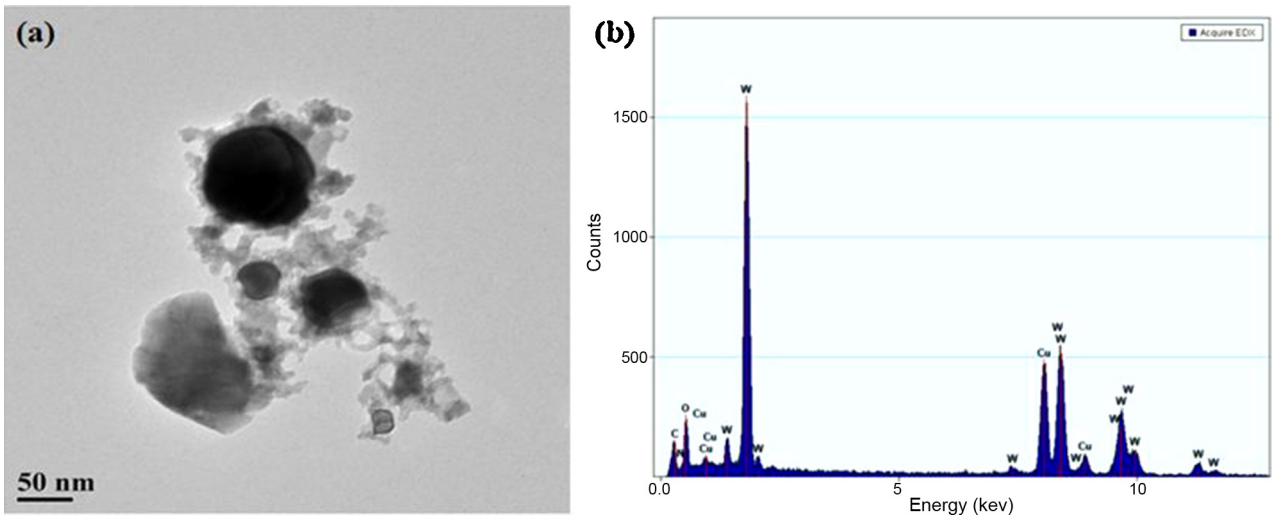

Fig. 1. (a) Tungsten nanoparticles of 80 nm and (b) EDX spectrum of the W NPs.

and Ojo (2009) suggest that the formation of a transient liquid phase (TLP) can lead to an enhanced homogeneous microstructure. This is possible by the insertion of an element to diffuse into the substrate material, which ultimately gives place to an isothermal solidification. The same beneficial effect is obtained by incorporating foils which contain nanoscale layers of Al and Ni that react exothermically as local heat sources for melting AuSn solder layers, as used by Wang et al. (2004). But, if the isothermal solidification is not complete, the liquid in the intermediate layer is solidified through eutectic phases during cooling, causing a decrease in the mechanical properties and corrosion strength of the weld bead, as shown by Yuan et al. (2012). Jang and Shih (2003) suggest that the metallic fillers containing silicon, boron or melting-point depressant solute with high solubility in the metal base, reduces the eutectic structures and diminishes the anomalous behavior at high-temperature. On the other hand, McGuire et al. (2009) established that tungsten reduces the size of borides and modifies the intermetallics; likewise, the effect of phase growth kinetics in stainless steels, by tungsten, has been confirmed by other authors (Park et al., 2006; Michalska and Sozańska, 2006; Kim et al., 1998).

In this context, this research work is aimed at modifying the brittle eutectic phase in the joining area of 304 stainless-steels, through a systematic study of incorporating tungsten nanoparticles (NPs) into microcracks, by the Brazing process.

2. Experimental procedure

2.1. Characterization and impregnation of tungsten NPs on the fractures of stainless steels

In order to study the brazing process and the effects of tungsten NPs (80 nm, Nanospyring), fractures were induced in 304 stainless steel rods of 10 × 60 mm by bending them with a mechanical testing machine; these fractures were inspected by scanning electron microscopy (SEM). Before conducting the brazing process, the tungsten NPs were characterized by transmission electron microscopy (TEM) and differential thermal analysis (DTA), at the rate of 10 °C/min. Characterization of tungsten NPs by DTA was carried out to study the phase transformations or thermal events as a function of brazing temperature without mixing with paste filler metal. The tungsten NPs were successively dispersed five times in ethanol, using a mixture of 0.5 g of tungsten NPs in 100 ml of ethanol, sonicated for 1 h. Separately, the steel fracture samples were ultrasonically cleaned with ethanol for 15 min to remove impurities of the microcracks and micropores and trapped air. Subsequently, the cleaned fracture samples were placed into the dispersed tungsten NPs and sonicated for 30 min. The sonication process promotes the incorporation of tungsten NPs into the microcrack fractures.

2.2. Brazing of fractured 304 stainless steel

In order to evaluate the effect of tungsten NPs in the brazing process of the stainless steel, the BNi-9 filler metal was characterized by the atomic absorption spectroscopy (AAS) method, and used in the fractured rods with and without tungsten NPs impregnation. The brazing process was conducted in a sealed tube furnace under an Ar gas flow of 0.1 L/min, the brazing temperature used was of 1200 °C for 10, 20, 30 and 60 min; the heating and cooling rates were fixed at 10 °C/min. The paste filler metal was spread on both types of fracture specimens, namely, those without and those with the dispersed tungsten NPs. This operation was followed by the manual joining of the fracture surface counterparts in such a way that the gap distance between the joined surfaces was close to 1 mm, which was measured with a Vernier and confirmed by optical microscopy. During the brazing tests, a soldering flux was not used because after fracturing, the samples were immediately cleaned and brazed, as described in this section. In order to determine the reactivity of the tungsten NPs on the stainless steel fractures, in another experiment, the impregnated fractures were exposed – without the paste filler metal – to the same brazing conditions (1200 °C for 1 h). The resulting samples were characterized by SEM and optical microscopy.

3. Results and discussion

3.1. Characterization of tungsten NPs and the effect in the brazing process

Fig. 1a is a TEM micrograph showing that the size of the tungsten NPs used to impregnate the stainless-steel fracture surfaces is less than 80 nm. Fig. 1b) is an EDX spectrum, revealing the W, Cu, O and C peaks of the elements constituting the NPs. The chemical composition of the filler metal is presented in Table 1.

Differential thermal analysis (DTA) conducted on the tungsten NPs in the temperature range between 1100 and 1200 °C

Table 1
Chemical composition of BNi-9 paste filler metal (wt%).

Element	B	Si	C	Fe	Na	Ca	Cr	Ni
wt%	2.57	0.041	1.16	0.35	0.14	0.22	16.32	Balance

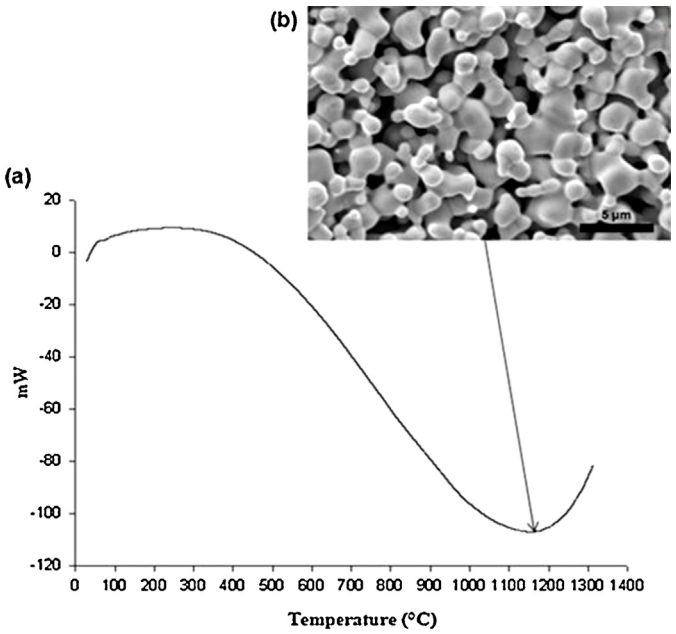

Fig. 2. (a) Differential thermal analysis of tungsten nanoparticles and (b) sintering of tungsten nanoparticles.

manifested an endothermic event (Fig. 2(a)) that can be associated with the sintering of the NPs. This fact is consistent with tests conducted at 1200 °C for 60 min in a flow of Ar, in tungsten NPs samples without the paste metallic filler. A representative SEM micrograph (Fig. 2(b)) supports the above statement, because particle size increase and neck formation amongst particles, are indication of the sintering phenomena, as shown by Richerson (1992).

The driving force for sintering corresponds to a decrease in the interfacial energy (γ) as established by Kingery et al. (1976):

$$\gamma = \left(\frac{\partial G}{\partial A}\right)_{T,P,n_i} \quad (1)$$

Eq. (1) represents the variation in the Gibbs free energy per unit area γ at constant temperature (T), pressure (P) and concentration of i species (n_i).

The liquid phase formed during sintering plays an important role, for it serves as a wetting agent and leads to particle (or grain) growth. Furthermore, the presence of small liquid amounts, together with the tungsten nanoparticles gives place to a capillary system in which a liquid rises and is spread if it wets the solid, namely, if the contact angle θ is less than 90° and the magnitude of the liquid–vapor surface tension (γ_{lv}) is favorably low, as a result of its balance with the solid–liquid (γs_l) and solid–vapor (γs_{lv}) interfacial energies. The nanoparticles impregnated into the microcracks can be thought of as countless capillary tubes through which the liquid phase can rise, in analogy with the tube-bundle theory, as presented in the work of Poirier and Geiger (1994). An expression for the threshold pressure, ΔP, needed to initiate incorporation of the liquid into the capillary tubes formed by the particles has been

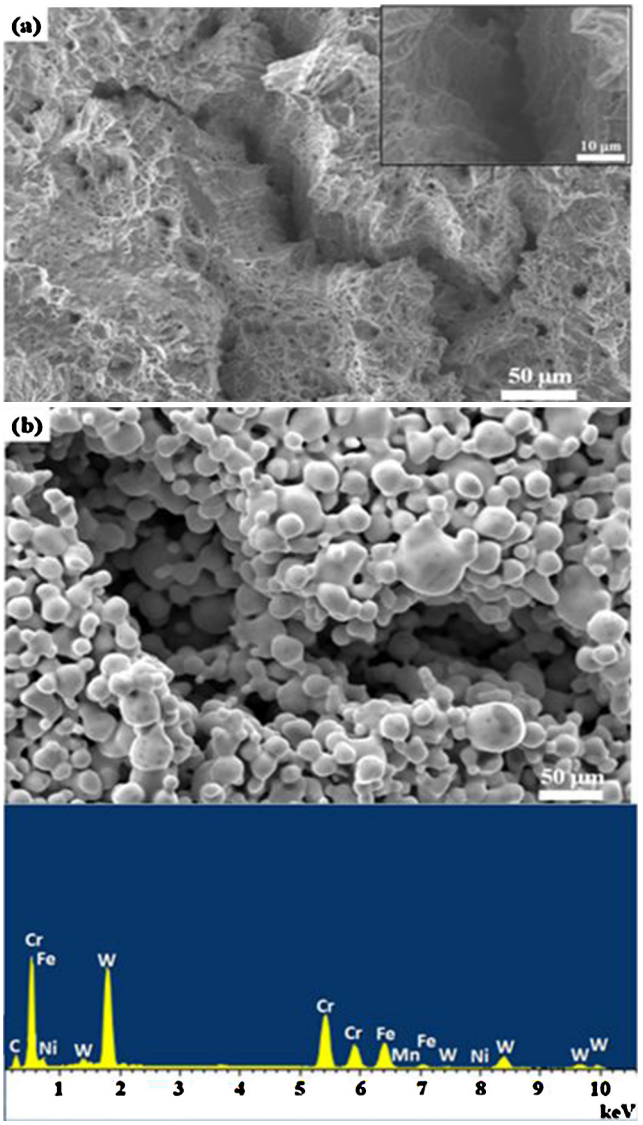

Fig. 3. SEM micrographs of the fractured surface of 304 stainless steel: (a) without tungsten NPs, the inset shows a zoom of a microcrack, (b) with tungsten NPs impregnation process after an annealing process at 1200 °C for 60 min and chemical analysis by EDX.

presented in the work of Pech-Canul and Makhlouf (2000), given as:

$$\Delta P = \frac{6\lambda\gamma lv\ \cos\theta(1-w)}{Dw} \quad (2)$$

where D is the average diameter of the particles, w is the void fraction in the porous body, λ is a geometry factor (usually taken as 1.4), and θ and γ_{lv} are the contact angle and the liquid–vapor surface tension, respectively. Similar to a pressureless infiltration system, if the liquid wets the solid phase – namely, if the contact angle θ is <90° – the capillary pressure (ΔP) will increase with decrease in particle size and the liquid will rise as in a capillary tube as proposed by Pech-Canul and Makhlouf (2000). Accordingly, the microcracks will be filled and sealed after solidification, preventing the restriction of the gap distance suggested from 0 to 1.5 mm (Wu et al., 2001). In the present analysis, it is postulated that the capillary vessels are formed by the nanoparticles impregnated and the microcracks themselves, in such a way that the filling of the microcracks by the liquid phase is the result of a synergistic effect developed both

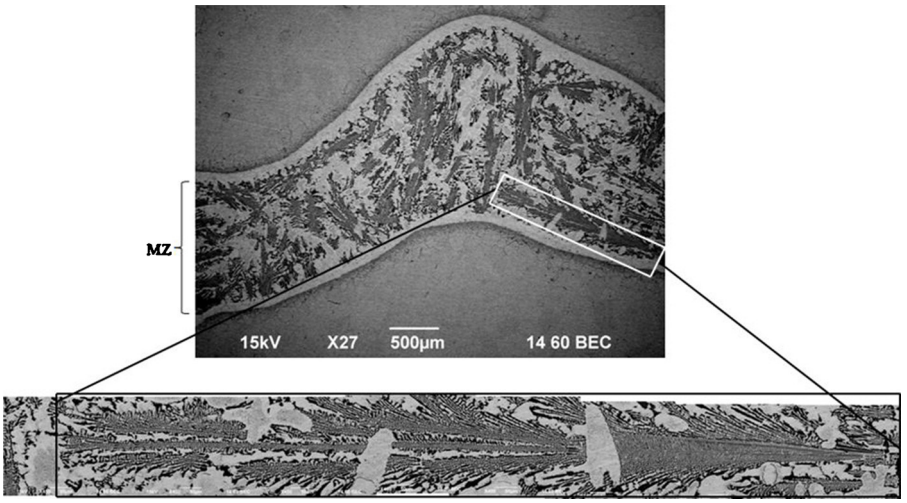

Fig. 4. Backscattered electron image of a so large eutectic in the weld bead without using tungsten NPs weld at 1200 °C for 60 min.

by the nanoparticles and the microcracks under thermodynamic wetting conditions.

3.2. Brazing of fractured 304 stainless steel

As a preliminary step to the brazing process, the behavior of tungsten NPs on the 304 stainless steel fractures was evaluated by SEM. Fig. 3 shows SEM micrographs of the fractured surface of 304 stainless steel before and after the tungsten NPs impregnation process. In Fig. 3(a), microcracks – between 10 and 160 μm in size – can be observed on the fractured surface, as well as micropores of varying sizes. Fig. 3(b) shows the result of the interaction of tungsten NPs with the stainless steel fracture surface after an annealing process at 1200 °C for 60 min. The growth of round-shaped tungsten particles on the stainless steel fracture surface can be seen. A remarkable observation is that tungsten particles grew both inside and outside the microcracks. The generation of spheres of larger sizes inside the microcracks may be ascribed to the sintering phenomena, according to the results obtained by DTA (Fig. 2(a)) in which the coalescence of particles can be seen in the depth of the microcracks. The composition of the bead is shown in the EDX spectrum (below Fig. 3(b)).

Fig. 4 shows a representative SEM image of the bonding region conducted without tungsten NPs impregnation; it can be observed that the MZ (melting zone) includes large lamellar-arborescent morphology structures (50–200 μm width × 300–600 μm long) which correspond to the eutectic, and small non-uniform structures which composition corresponds to Cr-boride (Fig. 5(a)). By contrast, as observed in Fig. 5(b), the tungsten NPs used in the brazing process promotes a noticeable change in the size, morphology and distribution of the structures in the MZ. When tungsten NPs are used, the lamellar eutectic structures are finer and uniformly dispersed in the MZ. To the best of the authors' knowledge, so far there is no consensus about the mechanism by which the eutectic microstructure becomes finer with the presence of tungsten nanoparticles, but it is generally accepted that during the dissolution step between the melting interlayer and the base metal, the tungsten nanoparticles act as a diffusion barrier for Cr, given that the eutectic phases are rich in this element. Moreover, some reports in the literature confirm that tungsten somehow modifies the morphology and size of phases (intermetallics, mainly) (Park et al., 2006; Michalska and Sozańska, 2006; Kim et al., 1998). The isothermal zone (ISZ), precipitation zone (PZ) and base metal (BM) remain apparently unmodified.

In order to investigate the role that play the tungsten NPs used in the brazing process on the mechanical properties, microhardness tests were performed in the bonding areas as a function of brazing time. Fig. 6 shows that due to the large eutectic regions in the samples without the addition of tungsten NPs, the microhardness tends to increase with brazing time, augmenting rapidly during the first 30 min, while only a relatively slow increase is observed between 30 and 60 min. By contrast, when tungsten NPs were used, because of a finer size of the eutectic structures and a resulting uniform distribution of boron in the MZ, the microhardness decreases as brazing time augments. A significant decrease

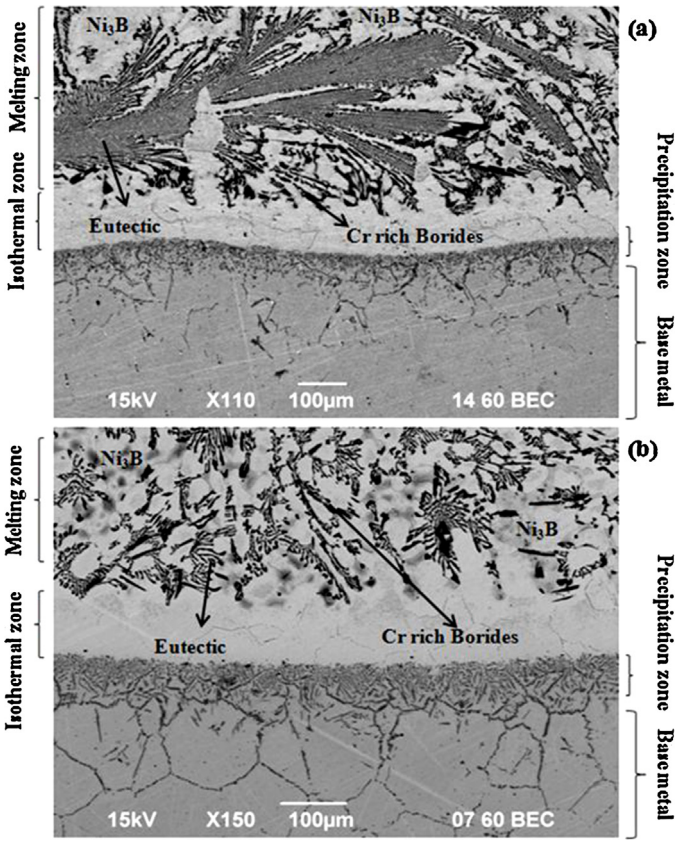

Fig. 5. Backscattered electron images of the weld bead in the stainless steel joined by brazing at 1200 °C for 60 min. (a) Without nanoparticles and (b) with nanoparticles.

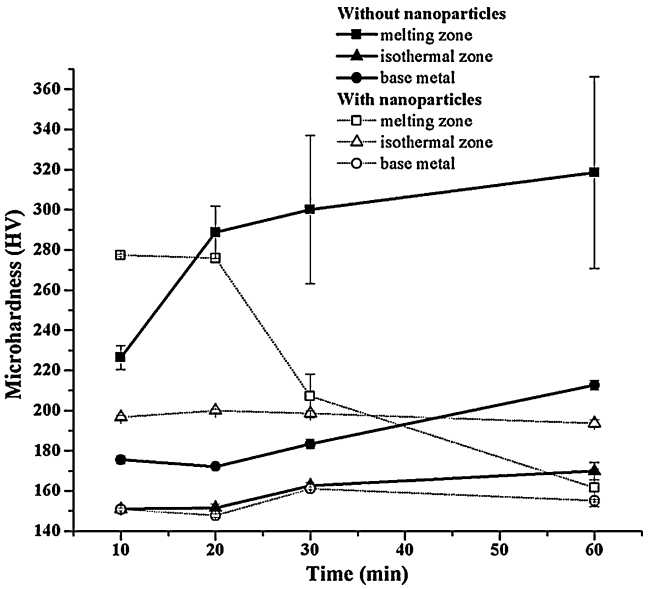

Fig. 6. Variation of the microhardness as function of brazing time in stainless steel samples brazed with and without tungsten nanoparticles.

of about 150 HV units can be obtained at the longest test time of 60 min, if the hardness values of the melting-zones of samples without and with addition of tungsten NPs are compared. Furthermore, a relatively constant microhardness can be observed between 30 and 60 min test time. The formation of large eutectic structures in the bonding zone gives rise to hard and brittle brazed joints that most likely will have deleterious effects upon the mechanical and corrosion-resistance properties, as showed by Chang et al. (2011). On the contrary and favorably, it is suggested in the literature (Wang et al., 2004) that higher strengths can be observed in the solder layers of reactive joints when finer microstructures are produced.

In the case of the isothermal zone, the effect is opposite because the microhardness increases slightly with incorporation of tungsten NPs. And like for the melting zone, in the isothermal zone, between 30 and 60 min test time, the microhardness becomes apparently constant. A possible explanation for the slight increase of Vickers microhardness in the isothermal zone is that a hardening effect occurs during cooling, associated to the fact that, as observed in Fig. 5(a) and (b), the ISZ of specimens with NPs is larger than that of specimens without nanoparticles.

It is worth noting that the microhardness of the base metal is essentially the same during all test times, both for samples with and without tungsten NPs additions, suggesting that there is no diffusion of any species into it and that nor the microstructure neither the mechanical properties are affected during the brazing process.

4. Conclusions

Within the framework of the experimental conditions used and the objective of this investigation, the following conclusions can be drawn:

- The microstructure in the joining zone is positively influenced in such a way that incorporation of the tungsten NPs leads to a finer eutectic microstructure with significantly lower microhardness as compared to that of samples without NPs. This is because tungsten can diminish the diffusion of Cr and avoid a larger eutectic.
- In specimens with tungsten NPs, the microhardness of the melting zone can be as low as half of that of samples evaluated without the nanoparticles.
- It is apparent that the microstructure of the base metal is not affected during the brazing process.
- It is postulated that the microcracks, together with the impregnated particles and the liquid phase form a capillary system in which, due to the wetting of the particles and microcrack surfaces by the liquid phase, after solidification and cooling to room temperature, the microstructure is characterized by a fine and uniform phase distribution, desirable for optimum mechanical behavior in service.

Acknowledgements

The authors wish to express their gratitude to the CONACYT and COMIMSA for supporting the development of the posdoctoral fellow of H. M. hdz-García with register number 98081. Likewise, the authors thank M.Sci. Lourdes Santiago Bautista for the preparation of metallographic samples.

References

Abdelfath, M.M., Ojo, O.A., 2009. On the extension of processing time with increase in temperature during transient-liquid phase bonding. Metall. Mater. Trans. A 40 (February), 377–385.
Byong-Ho, R., Dae-Up, K., 2002. Development of insert metal for transient liquid phase bonding of Fe-base heat resistant alloy. Met. Mater. Int. 8 (5), 427–433.
Chang, S.Y., Jain, C.C., Chuang, T.H., Feng, L.P., Tsao, L.C., 2011. Mater. Des. 32, 4720–4727.
Cook III, G.O., Sorensen, C.D., 2011. Overview of transient liquid phase and partial transient liquid phase bonding. J. Mater. Sci. 46, 5305–5323.
Jalilian, F., Jahazi, M., Drew, R.A., 2006. Microstructural evolution during transient liquid phase bonding of Inconel 617 using Ni–Si–B filler metal. Mater. Sci. Eng. A 423, 269–281.
Jang, J.S., Shih, H.P., 2003. Evolution of microstructure of AISI 304 stainless steel joint brazed by mechanically alloyed nickel base filler with different silicon content. J. Mater. Sci. Lett. 22, 79–82.
Kim, Sang-Beom, Paik, Kyung-Wook, Kim, Young-Gil, 1998. Effect of Mo substitution by W on high temperature embrittlement characteristics in duplex stainless steels. Mater. Sci. Eng. A 247, 67–74.
Kingery, W.D., Bowen, H.K., Uhlmann, D.R., 1976. Introduction to Ceramics, second ed. John Wiley & Sons, New York.
McGuire, D., Huang, X., Nagy, D., Chen, W., 2009. Effect of tungsten addition on the nucleation of borides in wide gap brazed joint. In: Proceedings of ASME Turbo Expo 2009: Power for Land, Sea and Air GT2009, Orlando, FL, USA, 8–12 June, pp. 1–9.
Michalska, J., Sozańska, M., 2006. Qualitative and quantitative analysis of σ and χ phases in 2205 duplex stainless steel. Mater. Charact. 56, 355–362.
Park, Chan-Jin, Ahn, Myung-Kyu, Kwon, Hyuk-Sang, 2006. Influences of Mo substitution by W on the precipitation kinetics of secondary phases and the associated localized corrosion and embrittlement in 29% Cr ferritic stainless steels. Materi. Sci. Eng. A 418, 211–217.
Pech-Canul, M.I., Makhlouf, M.M., 2000. Processing of Al–SiCp metal matrix composites by pressureless infiltration of SiCp preforms. J. Mater. Synth. Process. 8 (1), 35–53.
Philips, N.R., Levi, C.G., Evans, A.G., 2008. Mechanisms of microstructure evolution in an austenitic stainless steel bond generated using a quaternary braze alloy. Metall. Mater. Trans. A 39A, 142–149.
Poirier, D.R., Geiger, G.H., 1994. Transport Phenomena in Materials Processing. TMS, The Minerals, Metals and Materials Society, Warrendale, PA, USA.
Pouranvari, M., Ekrami, A., Kokabi, A.H., 2009. Effect of bonding temperature on microstructure development during TLP bonding of a nickel base superalloy. J. Alloys Compd. 469, 270–275.
Richerson, D.W., 1992. Modern Ceramic Engineering, Properties, Processing, and Use in Design, second ed. Marcel Dekker Inc., New York, USA.
Wang, J., et al., 2004. Joining of stainless-steel specimens with nanostructured Al/Ni foils. J. Appl. Phys. 95 (1), 248–256, http://dx.doi.org/10.1063/1.1629390.
Wu, X.W., Chandel, R.S., Seow, H.P., Li, H., 2001. Wide gap brazing of stainless steel to nickel-based superalloy. J. Mater. Process. Technol. 113, 215–221.
Yuan, X., Bok Kim, M., Ho Cho, Y., Yun Kang, Ch., 2012. Microstructures, mechanical and chemical properties of TLP-bonded joints in a duplex stainless steel with amorphous Ni-based insert alloys. Metall. Mater. Trans. A 43 (June), 1989–2001.
Zhou, Y., 2001. Analytical modeling of isothermal solidification during transient liquid phase (TLP) bonding. J. Mater. Sci. Lett. 20, 841–844.

InCites™ Journal Citation Reports®

THOMSON REUTERS™

JOURNAL OF MATERIALS PROCESSING TECHNOLOGY

ISSN: 0924-0136

ELSEVIER SCIENCE SA
PO BOX 564, 1001 LAUSANNE, SWITZERLAND
SWITZERLAND

Go to Journal Table of Contents Go to Ulrich's

Titles
ISO: J. Mater. Process. Technol.
JCR Abbrev: J MATER PROCESS TECH

Categories
ENGINEERING, INDUSTRIAL - SCIE;
ENGINEERING, MANUFACTURING - SCIE;
MATERIALS SCIENCE, MULTIDISCIPLINARY - SCIE;

Languages
ENGLISH

24 Issues/Year;

Key Indicators

Year	Total Cites Graph	Journal Impact Factor Graph	Impact Factor Without Journal Self Cites Graph	5 Year Impact Factor Graph	Immediacy Index Graph	Citable Items Graph	Cited Half-Life Graph	Citing Half-Life Graph	Eigenfactor Score Graph	Article Influence Score Graph
2013	19,574	2.041	1.862	2.328	0.360	247	8.5	8.4	0.02822	0.678
2012	18,426	1.953	1.733	2.176	0.332	295	7.8	8.3	0.03509	0.654
2011	16,633	1.783	1.688	1.881	0.421	242	7.3	7.7	0.03712	0.585
2010	15,777	1.570	1.502	1.730	0.267	273	6.6	8.0	0.03836	0.500